NANO LETTERS

Letter

pubs.acs.org/NanoLett

Nanostructured Holograms for Broadband Manipulation of Vector Beams

Jiao Lin,[†,‡] Patrice Genevet,[†] Mikhail A. Kats,[†] Nicholas Antoniou,[§] and Federico Capasso*[,†]

[†]School of Engineering and Applied Sciences, Harvard University, Cambridge, Massachusetts 02138, United States

[‡]Singapore Institute of Manufacturing Technology, 71 Nanyang Drive, Singapore 638075, Singapore

[§]Center for Nanoscale Systems, Harvard University, Cambridge, Massachusetts 02138, United States

ABSTRACT: We report a new type of holographic interface, which is able to manipulate the three fundamental properties of light (phase, amplitude, and polarization) over a broad wavelength range. The design strategy relies on replacing the large openings of conventional holograms by arrays of subwavelength apertures, oriented to locally select a particular state of polarization. The resulting optical element can therefore be viewed as the superposition of two independent structures with very different length scales, that is, a hologram with each of its apertures filled with nanoscale openings to only transmit a desired state of polarization. As an implementation, we fabricated a nanostructured holographic plate that can generate radially polarized optical beams from circularly polarized incident light, and we demonstrated that it can operate over a broad range of wavelengths. The ability of a single holographic interface to simultaneously shape the amplitude, phase, and polarization of light can find widespread applications in photonics.

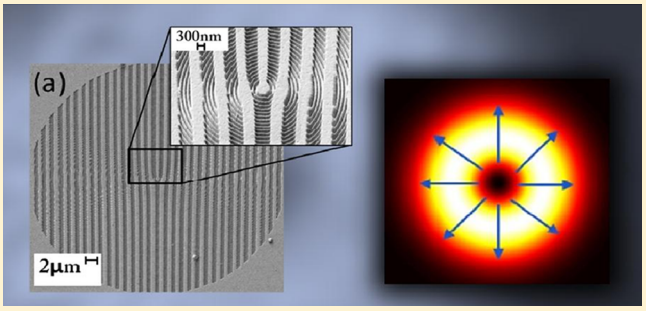

KEYWORDS: *Nanophotonics, metamaterials, metasurfaces, holography, detour-phase holograms, vector beams*

Optical elements such as lenses, phase plates, and polarizers, including diffractive components, independently control the *amplitude*, *phase*, and *state of polarization* of light so that multiple cascaded optical elements are needed for vector beam manipulation. The ultimate challenge for manipulating a light beam is therefore the control of the vector field with a single optical element, that is, of the spatial distribution of amplitude, phase, and state of polarization. A few techniques,[1−4] such as detour-phase holograms, achieve both amplitude and phase modulation with a single component.

With the advent of nanophotonics, we have witnessed the development of new types of optical interfaces, or metasurfaces, that can introduce phase jumps along the light path to manipulate phase, amplitude, and eventually the polarization of light over subwavelength propagation distances.[5−11] The working principle employs nanoscale optical resonators patterned at the interface at specific positions and with designed plasmonic resonances to engineer the scattering properties of the whole interface. The complexity in the design of each scattering element and the relatively narrow operating bandwidth of such metasurfaces prompted us to find more convenient approaches for controlling light. Combining concepts of nanophotonics with the principle of detour-phase holography, we propose a radically different type of interface which, after being designed initially for a given wavelength, can manipulate phase amplitude and polarization over a significant spectral region. *The novelty lies in replacing the large openings of conventional holograms by arrays of subwavelength apertures, oriented to locally select a particular state of polarization.* The resulting design can therefore be viewed as the superposition of two independent structures with very different length scales, that is, a detour-phase hologram with each of its apertures filled with nanoscale openings to transmit only a desired state of polarization.

We would like to start our discussion with the concept of a traditional detour-phase hologram,[1,12] which can be understood by first considering an infinite one-dimensional structure made of periodically repeated apertures of width αW with a period W, where $\alpha \leq 1$. The transmittance function in the plane in $z = 0$ of this structure is given by:

$$T(x) = \left(\sum_n \delta_D(x - nW)\right) * \prod\left(\frac{x}{\alpha W}\right) \quad (1)$$

where δ_D is the delta dirac function, the asterisk denotes convolution and $\prod$ denotes the "top hat" function. The diffraction pattern of this function is given, in the paraxial approximation, by:

$$f(\theta) = \frac{e^{-jkz}}{j\lambda z}\hat{T}\left(\frac{\sin(\theta)}{\lambda}\right) \quad (2)$$

Received: June 4, 2013
Revised: July 30, 2013
Published: August 5, 2013

   dx.doi.org/10.1021/nl402039y | *Nano Lett.* 2013, 13, 4269−4274

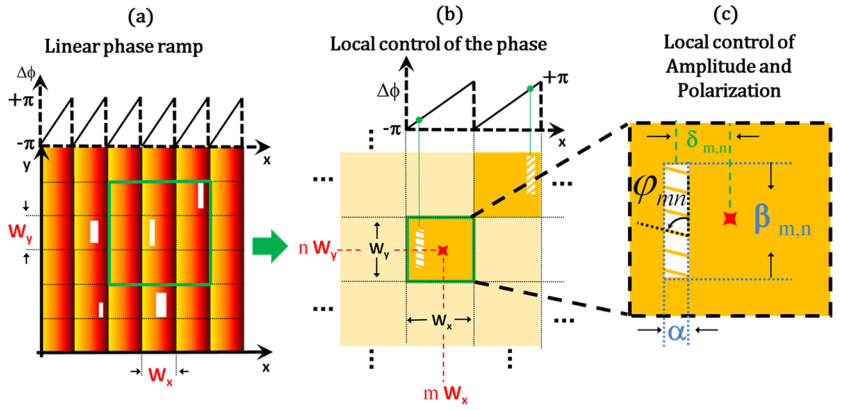

Figure 1. General description of an optical component to control simultaneously amplitude, phase, and polarization of a vector field. (a) Illustration of the concept of the detour phase: Consider a monochromatic plane wave incoming at normal incidence and transmitted through the apertured interface, from the shift theorem of Fourier optics, an aperture shifted by δ_{nm} from the center of the (m,n)th pixel creates a phase shift given by $2\pi\delta_{nm}[x/(\lambda z)] = 2\pi(\delta_{nm}/\lambda)\sin(\theta)$; i.e., an interface seen by an observer standing at an angle θ from the normal can be discretized by sections of width $W_x = \lambda/\sin(\theta)$, each of which can then be apertured to select a phase within the 2π range. Conventional detour-phase holograms are composed of many pixels, each scattering light with a given phase delay. (b) The overall complex amplitude of light emerging through each pixel is modulated by controlling both the position and the size of the slit in the pixel. The width of the apertures, α, is kept constant across the interface. The amount of light passing through the pixel at (mW_x, nW_y) is proportional to the length of the aperture $\beta_{m,n}$. The aperture x-position within the pixel $(\delta_{m,n})$ controls the phase of the light transmitted through the (n, m)th pixel. Schematics (a) and (b), without the subwavelength apertures, describe a conventional detour-phase hologram. (c) By decorating each aperture with subwavelength features to form a wire-grid polarizer oriented at some angle $\varphi_{n,m}$, we can locally convert a generic state of polarization (i.e., elliptical) of incident polarization into a specific state of polarization of the scattered radiation. For linear apertures with a large aspect ratio, the selected polarization is linear.

where the caret symbol (^) denotes the Fourier transform and z is the direction normal to the hologram. By shifting the periodic function along the lateral dimension x by an amount of δ, that is, $T = T(x - \delta)$, the shift theorem of Fourier optics implies that the nonzero diffraction orders experience a phase oscillation equal to $e^{2j[\pi\delta(\sin(\theta))/\lambda]}$.[12] This factor is easily understood physically by noting that waves diffracted by adjacent slits give rise to intensity maxima in a direction θ if their path difference along θ is an integer number of wavelengths. Detour-phase holograms,[1,12] which are basically apertures etched in opaque films, use this property to encode phase and amplitude of the wavefront. The apertures are disposed along the x direction in the $z = 0$ plane, at locations δ to select the desired phase shifts; see Figure 1a. Note that, at an angle θ_1, the phase shift for a given wavelength (λ_1) will be observed at another wavelength (λ_2) at the angle θ_2 defined by $\theta_2 = \sin^{-1}[(\lambda_2/\lambda_1)\sin\theta_1]$.

To this method of manipulating phase and amplitude (which is controlled by the size of the apertures) we add control over the spatial distribution of the *polarization* by including subwavelength structures within the apertures of the detour-phase hologram, as illustrated in Figure 1.

Given an incident beam with a generic state of polarization (i.e., elliptical) incident on a 2D apertured interface, the transmitted field distribution is $\vec{E}_{z=0^+}(x, y) = \vec{E}_{z=0^-}(x, y)T(x, y)$ where $z = 0^+$ and $z = 0^-$ represent the location just ahead and just behind an interface represented by a transmittance function $T(x,y)$.

Assuming an incident circularly polarized beam:

$$\vec{E}_{cp} = \vec{e}_x + j\vec{e}_y = e^{j\theta}(\vec{e}_r + j\vec{e}_\theta) \tag{3}$$

the transmittance $T(x,y)$ in vectorial form reads:

$$T(x, y) = \left[\sum_{n,m} \delta_D(x - nW_x - \delta_{nm}, y - mW_y)\right] * \prod\left(\frac{x}{\alpha W_x}, \frac{y}{\beta_{nm} W_y}\right) \times \begin{bmatrix} \cos\varphi_{mn} \\ \sin\varphi_{mn} \end{bmatrix} \tag{4}$$

The parameters α and β_{mn}, which represent the size of the opening along x and y within a single cell, control the modulation of the amplitude and the phase. In particular, the local phase shift at the pixel (m,n) is given by $\varphi_{m,n} = (2\pi\delta_{mn}/W_x)$, and the amplitude increases monotonically with increasing β_{mn}. It is important to point out that the width of the slit in the x-direction, noted α in Figure 1c, not only affects the transmitted amplitude but also affects the precision with which the phase is specified. Precise phase selection ideally requires very narrow slits, which, in practice, considerably decreases the amount of light transmitted through each pixel. In our experiments, a compromise is reached for $\alpha/W_x = 0.5$, that is, when half of the area of the element is transparent, as previously demonstrated for binary holograms.[13]

In the following, we discuss a particular implementation of these nanostructured holograms to create a radially polarized beam from an incident circularly polarized Gaussian beam. Polarization is a property of the electromagnetic field that arises from its vector nature and plays an indispensable role in a wide range of optical phenomena and applications.[14−17] These exemplary studies consider light with a spatially homogeneous state of polarization, also called scalar fields, for which the propagation is entirely described by the *scalar* Helmholtz equation. Light with an inhomogeneous polarization state, that is, a spatially varying polarization distribution in the transverse beam cross-section, represents a more general scenario that has started to open up new research opportunities in optics. Significant efforts have been devoted to the creation of cylindrical vector beams (CVBs), a family of solutions of the more general vector wave equation,[18] which features a

dx.doi.org/10.1021/nl402039y | Nano Lett. 2013, 13, 4269−4274

cylindrical state of polarization in the dimension transverse to the propagation direction.[19] CVBs are familiar objects in electromagnetic waveguide theory and are often encountered in metallic waveguides with cylindrical boundary conditions[20] or in optical fibers.[21] One can also directly produce free-space CVBs from lasers by imposing an appropriate transverse mode selection mechanism.[22]

The radially polarized beam (RPB) is the most widely used free-space CVB (Figure 2). Due to complete radial symmetry in their transverse field, including the polarization state, RPBs have potential for applications in imaging,[23−25] optical trapping,[26−28] and laser machining.[29−31] It is often convenient to decompose CVBs into the superposition of solutions of the Helmholtz equation in two orthogonal spatially homogeneous polarization states. With this approach, an RPB can be obtained from the superposition of two cross-polarized Hermite−Gauss (HG) modes (Figure 2b and c).[32−34] Other proposals for the generation of RPBs includes selective coupling of free space light to specific transverse modes in a multimode optical fiber,[35] in a THz metallic waveguide[36] or in a laser cavity.[22,37] More compact converters make use of birefringent materials with spatially varying orientation of the optical axes.[23,38−40] A radial polarizer, which consists of subwavelength circular metallic gratings (Figure 2a),[41] has recently been used to generate a RPB from a circularly polarized input beam.[42] However, spatial control of the polarization state of a beam in this manner inevitably introduces unwanted spatially varying phase distributions, known to be a manifestation of the Pancharatnam−Berry (P−B) phase.[43−45] Therefore, attempts to convert a circularly polarized beam into a RPB by using a radial polarizer yields a far-field intensity pattern that deviates from the desired doughnut-shaped RPB (Figure 3a).

The additional phase imparted to a light beam in the process of polarization conversion from a circularly polarized beam to a radially polarized one using a radial polarizer has a spiral distribution $e^{j\theta}$.[45] The origin of this spiral phase is the projection of incident light with, for example, right-handed circular polarization (eq 3) onto the state of polarization of the light passing through a circular wire-grid polarizer, that is, the radial state of polarization, such that the output beam profile can be described by:

$$\vec{E}_{\text{out}} = e^{j\theta}\vec{e}_r \tag{5}$$

The P−B phase term, $e^{j\theta}$, is often compensated by additional optical elements, for example, spiral phase plates[46] that impose a conjugate spiral phase $e^{-j\theta}$, that is, with the helicity of wavefront reversed with respect to the unwanted P−B phase. A different approach to introduce such a spiral phase distribution involves diffracting the light from a binary fork hologram (Figure 3b), which achieves phase modulation in the diffracted orders.[47,48] The design of such a fork hologram is performed by calculating the off-axis interference pattern between an object beam (a vortex beam carrying the spiral phase in our case) and a reference beam (usually a Gaussian beam). This interferometric approach has been recently used to design plasmonic interfaces which facilitate the selective detection of light carrying orbital angular momentum.[49] As mentioned in the introduction, the novelty of our approach relies in replacing the large openings of holograms by arrays of subwavelength apertures, oriented to locally select a particular state of polarization. To avoid spurious diffraction effects from these polarizing metallic apertures, their size is chosen to be significantly smaller than the wavelength of light. The resulting design can therefore be viewed as a superposition of two independent structures with very different length scales. The larger scale features, as presented in Figure 3b, are spaced by roughly $\lambda/\sin\theta$, where θ is the first order diffraction angle for normal incidence; these control the spatial modulation of the phase. The smaller features can be viewed as miniature wire-grid polarizers, which locally control the state of polarization of the transmitted light. To generate a RPB, the fork hologram creates a spiral phase front, and the subwavelength apertures

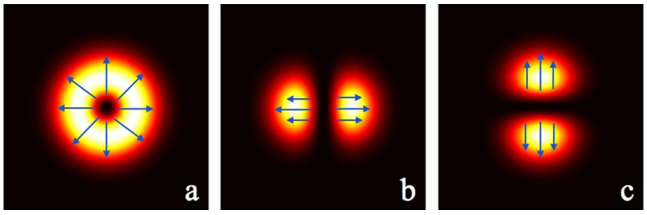

Figure 2. (a) Hollow intensity distribution of a typical radially polarized beam (RPB). The RPB mode can be decomposed into a linear combination of two orthogonal *x*- and *y*-polarized HG_{10} modes. The intensity distribution of the HG_{10} modes are shown in b and c. The blue arrows indicate the state of polarization.

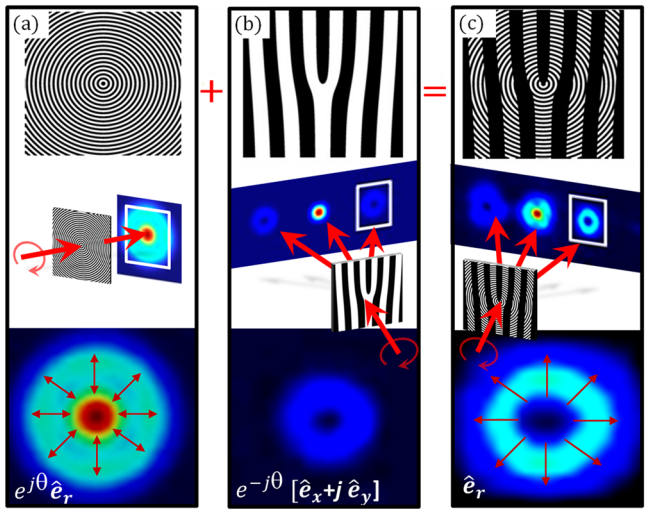

Figure 3. The technique used to generate radially polarized beams (RPBs) combines subwavelength apertures for polarization control and wavelength-scale diffracting apertures. The structure that generates RPBs (c) is the superposition of a radial polarizer (a) and a fork diffraction hologram (b) to cancel the $e^{j\theta}$ phase contribution that arises from the projection of the circularly polarized optical field onto the state of radial polarization, as explained in the text. The black and white colors in the upper row represent respectively "0" (opaque) and "1" (transparent) in the transmittance function of the device. The periods in a and b are 200 nm and 1.2 μm, respectively. For each panel, the figure in the middle presents the far-field intensity distribution after traversing the structure with the transmittance function given by the upper part of the panel. The simulated interfaces comprise patterned Au films (150 nm thick) on a glass substrate. The calculated far-field intensity distributions presented in the lower part of each panel are enlarged versions of the diffracted beams located in the white boxes. Each sample is illuminated by a right-handed circularly polarized plane wave incoming at normal incidence. The wavelength of the light in the simulation is 633 nm, but identical results have been obtained across the visible spectrum. All simulations have been performed using commercial finite-difference time-domain (FDTD) software.

dx.doi.org/10.1021/nl402039y | *Nano Lett.* 2013, 13, 4269−4274

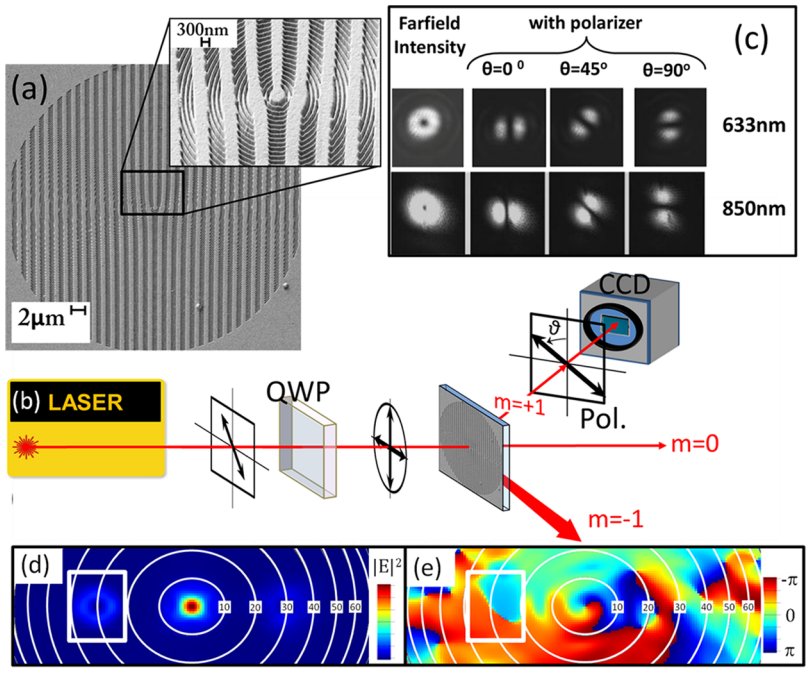

Figure 4. The fabricated structure (a) was tested with two different wavelengths (633 and 850 nm). A quarter wave plate converts the linearly polarized laser beam to a circularly polarized one. The far-field distribution is captured by a CCD camera after passing through a linear analyzer oriented at varying angles. (a) SEM micrograph of the device; (b) the experimental setup; (c) measured far-field intensity distributions at two wavelengths, without and with analyzer, the latter oriented at different angles in front of the CCD camera. These intensity patterns demonstrate that the $m = +1$ beam is radially polarized and that the device is broadband. Note that the sample creates several diffraction orders; due to the subwavelength patterning, the $m = -1$ order acquires an additional orbital angular momentum, leading to an overall $e^{j2\theta}$ phase factor. (d and e) Far-field intensity and phase profiles plotted in polar coordinates at 1 m away from the interface calculated from the transmitted near-fields 150 nm behind the nanostructured hologram, assuming a free-standing interface. The doughnut intensity distribution of the radial beam is associated with a relatively flat phase front (white rectangle).

select the radial state of polarization. For incident light with circular polarization, the overall effect of the structure is to generate a radially polarized beam without the need for an additional P−B phase compensation element, Figure 3c. For fabrication convenience, we are considering here only the binary version of the hologram, consisting of wavelength-scale openings in an optically opaque gold (Au) film deposited on a SiO_2 substrate. Although these holograms are designed to create a virtual image at a given angle for a specific wavelength, they actually operate over a broad wavelength range, creating virtual images at the corresponding angles. Therefore, any device designed by combining wavelength and subwavelength scale apertures will operate over a broad wavelength range so long as the apertures are nonresonant. The bandwidth comprises wavelengths that are longer than the physical size of the smaller apertures and shorter than the period of the holograms, though the resulting beams appear at different angles, depending on the wavelength, as predicted by the grating equation.

To demonstrate our technique, we fabricated a binary flat optical component to generate an RPB from a circularly polarized Gaussian beam by ion milling the pattern shown in Figure 3c, using a focused ion beam (Zeiss NVision 40), into a 150 nm thick Au film deposited by electron beam evaporation onto a glass substrate (Figure 4a). The period of the subwavelength apertures is 200 nm, and the size of the features forming the hologram is approximately 1.25 μm. As shown in Figure 4b, our sample was illuminated by circularly polarized laser beams at two different wavelengths (633 and 850 nm). The diffraction order that carries the RPB ($m = +1$) was directed through a linear polarizer, and its intensity distribution was captured by a CCD camera. By rotating the linear polarizer in front of the beam with the characteristic doughnut intensity profile ($m = +1$ diffraction order), we demonstrated that its polarization is oriented radially, in agreement with Figure 2. As expected from the design, radially polarized beams at 633 and 850 nm are generated at angles of about 32° and 45°, respectively. For both wavelengths, the RPBs exhibit similar quality and characteristics, revealed by rotating the linear polarizer around the beam axis as in Figure 4c. The slight discrepancies in the shape of the intensity distribution for the two wavelengths are due to the finite aperture of the lens used to image the beams on the CCD camera. The devices proposed in this Letter are still related to traditional detour-phase holograms: only one (defined as $m = +1$) of the two first diffraction orders carries the desired amplitude, phase, and polarization which gives rise to the RPB. Similar to Leith−Upatnieks holograms,[50] a twin image with conjugate phase modulation exists in the other first order. This second beam carries a phase factor $e^{2j\theta}$ corresponding to an additional angular momentum acquired in scattering off the holographic grating. Figure 4d and e is the simulated far-field intensity and phase profiles. Note that the zero diffraction order, also radially polarized, presents a nonvanishing topological charge which cancels for the $m = 1$ order (as expected for a RPB, white rectangle). The simulated overall transmission efficiency of the interface is about 19% at 633 nm. This number accounts for the absorption in the metal, including the three diffraction orders. From the far-field intensity distribution, we calculated the normalized power in a cone centered on the radial beam axis

dx.doi.org/10.1021/nl402039y | Nano Lett. 2013, 13, 4269−4274

defined by a half angle of 15°, and we obtained a RPB conversion efficiency of about 3.95%. In this configuration, about 4% of the incident power is lost in the $m = -1$ diffraction order. It is possible to considerably increase the RPB conversion efficiency by adding the proper linear phase gradient on the designed phase profile, that is, creating a nanostructured hologram blazed at the first diffraction order. As we discussed in the manuscript, the purpose of the nanostructures is to filter a given state of polarization. Thus, even a perfect nanostructured hologram will only transmit 50% of an unpolarized input beam. The transmission efficiency of light with a well-defined incident polarization will therefore depend on the desired state of polarization of the transmitted light. Imperfections in the nanostructures such as accidental scattering sites and material defects reduce the hologram contrast and might also reduce the throughput efficiency.

In conclusion, we have revisited the concept of detour-phase holograms by incorporating apertures with subwavelength features. These features extend the functionality of conventional printable wavelength-scale binary holograms, which can manipulate complex scalar fields, to include control of the polarization of light. By incorporating subwavelength features, we have achieved full control of vector optical field over a broad range of wavelengths with a single flat subwavelength binary structure. The design approach proposed in this Letter for modulating a vector beam is more than just a simple superposition (as it might appear) of wire grid polarizers to conventional detour-phase holograms. Phase modulation and polarization modulation are not independent features that can be simply added on each other. As shown for the generation of RPBs, the P−B phase induced by the projection of the incident polarization onto the desired state of polarization plays an important role and has to be determined in advance, before designing the holograms. The detour phase which is defined by the position of the aperture in each pixel has to be equal to the difference between the desired phase modulation and the P−B phase. The ability to appropriately shape amplitude, phase, and polarization of light with a single ultrathin interface gives an incentive for the generation of more complex light fields such as high-order Bessel, Mathieu, or Airy beams and promises revolutionary advances in the fields of integrated photonics, optical trapping,[51] or quantum optics.[52]

AUTHOR INFORMATION

Corresponding Author

*E-mail: capasso@seas.harvard.edu.

Author Contributions

J.L. and P.G. contributed equally to this work.

Notes

The authors declare no competing financial interest.

ACKNOWLEDGMENTS

The authors thank Y. Yao, J. P. B. Mueller, and R. Blanchard for discussions. This research is supported in part by the Air Force Office of Scientific Research under grant number FA9550-12-1-0289. M.A.K. is supported by the National Science Foundation through a Graduate Research Fellowship. J.L. also acknowledges the support from the Agency for Science, Technology and Research (A*STAR), Singapore. Fabrication of the devices was carried out at the Center for Nanoscale Systems (CNS) at Harvard University, a member of the National Nanotechnology Infrastructure Network (NNIN), which is supported by the NSF (under award no. ECS-0335765).

REFERENCES

(1) Brown, B. R.; Lohmann, A. W. Complex spatial filtering with binary masks. *Appl. Opt.* **1966**, *5*, 967−969.

(2) Hariharan, P. *Optical Holography: Principles, Techniques and Applications*; Cambridge University Press: New York, 1996.

(3) Davis, J. A.; Cottrell, D. M.; Campos, J.; Yzuel, M. J.; Moreno, I. Encoding amplitude information onto phase-only filters. *Appl. Opt.* **1999**, *38*, 5004−5013.

(4) Arrizón, V. Complex modulation with a twisted-nematic liquid-crystal spatial light modulator: double-pixel approach. *Opt. Lett.* **2003**, *28*, 1359−1361.

(5) Yu, N.; Genevet, P.; Kats, M. A.; Aieta, F.; Tetienne, J.-P.; Capasso, F.; Gaburro, Z. Light propagation with phase discontinuities: Generalized laws of reflection and refraction. *Science* **2011**, *334*, 333.

(6) Ni, X.; Emani, N. K.; Kildishev, A. V.; Boltasseva, A.; Shalaev, V. M. Broadband Light Bending with Plasmonic Nanoantennas. *Science* **2012**, *335*, 427.

(7) Genevet, P.; Yu, N.; Aieta, F.; Lin, J.; Kats, M. A.; Blanchard, R.; Scully, M. O.; Gaburro, Z.; Capasso, F. Ultra-thin plasmonic optical vortex plate based on phase discontinuities. *Appl. Phys. Lett.* **2012**, *100*, 13101.

(8) Aieta, F.; Genevet, P.; Yu, N.; Kats, M. A.; Gaburro, Z.; Capasso, F. Out-of-Plane Reflection and Refraction of Light by Anisotropic Optical Antenna Metasurfaces with Phase Discontinuities. *Nano Lett.* **2012**, *12* (3), 1702−1706.

(9) Yu, N.; Aieta, F.; Genevet, P.; Kats, M. A.; Gaburro, Z.; Capasso, F. A Broadband, Background-Free Quarter-Wave Plate Based on Plasmonic Metasurfaces. *Nano Lett.* **2012**, *12*, 6328.

(10) Pors, A.; Nielsen, M. G.; Lynge Eriksen, R.; Bozhevolnyi, S. I. Broadband Focusing Flat Mirrors Based on Plasmonic Gradient Metasurfaces. *Nano Lett.* **2013**, *13* (2), 829−834.

(11) Yu, N.; Genevet, P.; Aieta, F.; Kats, M. A.; Blanchard, R.; Aoust, G.; Tetienne, J. P.; Gaburro, Z.; Capasso, F. Flat photonics: Controlling wavefronts with optical antenna metasurfaces. *IEEE Sel. Top. Quantum Electron.* **2013**, *19*, 4700423.

(12) Goodman, J. W. *Introduction to Fourier Optics*, 2nd ed.; McGraw-Hill: New York, 1996.

(13) Lohmann, A. W.; Paris, D. P. Binary Fraunhofer holograms generated by computer. *Appl. Opt.* **1967**, *6*, 1739−1748.

(14) Kliger, D. S.; Lewis, J. W.; Randall, C. E. *Polarized light in optics and spectroscopy*; Academic Press: New York, 1990).

(15) Damask, J. N. *Polarization optics in telecommunications*; Springer: New York, 2004.

(16) Tuchin, V. V.; Wang, L. V.; Zimnyakov, D. A. *Optical polarization in biomedical applications*; Springer: New York, 2006.

(17) Svirko, Yu. P.; Zheludev, N. I. *Polarization of light in nonlinear optics*; John Wiley & Sons: Wiley, 1998.

(18) Hall, D. G. Vector-beam solutions of Maxwell's wave equation. *Opt. Lett.* **1996**, *21*, 9−11.

(19) Zhan, Q. Cylindrical vector beams: from mathematical concepts to applications. *Adv. Opt. Photonics* **2009**, *1*, 1−57.

(20) Harrington, R. F. *Time-Harmonic Electromagnetic Fields*; McGraw-Hill: New York, 1961; p 207.

(21) Okamoto, K. *Fundamentals of Optical Waveguides*, 2nd ed.; Academic Press: New York, 2006; p 74.

(22) Pohl, D. Operation of a Ruby laser in the purely transverse electric mode TE_{01}. *Appl. Phys. Lett.* **1972**, *20*, 266−267.

(23) Dorn, R.; Quabis, S.; Leuchs, G. Sharper focus for a radially polarized light beam. *Phys. Rev. Lett.* **2003**, *91*, 233901.

(24) Sheppard, C. J. R.; Choudhury, A. Annular pupils, radial polarization, and superresolution. *Appl. Opt.* **2004**, *43*, 4322−4327.

(25) Wang, H. F.; Shi, L. P.; Lukyanchuk, B.; Sheppard, C.; Chong, C. T. Creation of a needle of longitudinally polarized light in vacuum using binary optics. *Nat. Photonics* **2008**, *2*, 501−505.

(26) Zhan, Q. Trapping metallic Rayleigh particles with radial polarization. *Opt. Express* **2004**, *12*, 3377−3382.

(27) Kawauchi, H.; Yonezawa, K.; Kozawa, Y.; Sato, S. Calculation of optical trapping forces on a dielectric sphere in the ray optics regime produced by a radially polarized laser beam. *Opt. Lett.* **2007**, *32*, 1839−1841.
(28) Zhao, Y. Q.; Zhan, Q.; Zhang, Y. L.; Li, Y. P. Creation of a three-dimensional optical chain for controllable particle delivery. *Opt. Lett.* **2005**, *30*, 848−850.
(29) Niziev, V. G.; Nesterov, A. V. Influence of beam polarization on laser cutting efficiency. *J. Phys. D* **1999**, *32*, 1455−1461.
(30) Kraus, M.; Ahmed, M. A.; Michalowski, A.; Voss, A.; Weber, R.; Graf, T. Microdrilling in steel using ultrashort pulsed laser beams with radial and azimuthal polarization. *Opt. Express* **2010**, *18*, 22305−22313.
(31) Lou, K.; Qian, S.-X.; Wang, X.-L; Li, Y.; Gu, B.; Tu, C.; Wang, H.-T. Two-dimensional microstructures induced by femtosecond vector light fields on silicon. *Opt. Express* **2012**, *20*, 120−127.
(32) Novotny, L.; Hecht, B. *Principles of Nano-Optics*; Cambridge University Press: New York, 2006.
(33) Tidwell, S. C.; Ford, D. H.; Kimura, W. D. Generating radially polarized beams interferometrically. *Appl. Opt.* **1990**, *29*, 2234−2239.
(34) Niziev, V. G.; Chang, R. S.; Nesterov, A. V. Generation of inhomogeneously polarized laser beams by use of a Sagnac interferometer. *Appl. Opt.* **2006**, *45*, 8393−8399.
(35) Volpe, G.; Petrov, D. Generation of cylindrical vector beams with few-mode fibers excited by Laguerre-Gaussian beams. *Opt. Commun.* **2004**, *237*, 89−95.
(36) Grosjean, T.; Baida, F.; Adam, R.; Guillet, J.-P.; Billot, L.; Nouvel, P.; Torres, J.; Penarier, A.; Charraut, D.; Chusseau, L. Linear to radial polarization conversion in the THz domain using a passive system. *Opt. Express* **2008**, *16*, 18895−18909.
(37) Ahmed, M. A.; Voss, A.; Vogel, M. M.; Graf, T. Multilayer polarizing grating mirror used for the generation of radial polarization inYb:YAG thin-disk lasers. *Opt. Lett.* **2007**, *32*, 3272−3274.
(38) Machavariani, G.; Lumer, Y.; Moshe, I.; Meir, A.; Jackel, S. Spatially-variable retardation plate for efficient generation of radiallyand azimuthally-polarized beams. *Opt. Commun.* **2008**, *281*, 732−738.
(39) Bomzon, Z.; Biener, G.; Kleiner, V.; Hasman, E. Radially and azimuthally polarized beams generated by space-variant dielectric subwavelength gratings. *Opt. Lett.* **2002**, *27*, 285−287.
(40) Lim, B. C.; Phua, P. B.; Lai, W. J.; Hong, M. H. Fast switchable electro-optic radial polarization retarder. *Opt. Lett.* **2008**, *33*, 950−952.
(41) Ahn, S.-W.; Lee, K.-D.; Kim, J.-S.; Kim, S. H.; Park, J.-D.; Lee, S.-H.; Yoon, P.-W. Fabrication of a 50nm half-pitch wire grid polarizer using nanoimprint lithography. *Nanotechnology* **2005**, *16*, 1874−1877.
(42) Ghadyani, Z.; Vartiainen, I.; Harder, I.; Iff, W.; Berger, A.; Lindlein, N.; Kuittinen, M. Concentric ring metal grating for generating radially polarized light. *Appl. Opt.* **2011**, *50*, 2451−2457.
(43) Pancharatnam, S. Generalized theory of interference, and its applications. *Proc. Ind. Acad. Sci. A* **1956**, *44*, 247−262.
(44) Berry, M. V. Quantal phase factors accompanying adiabatic changes. *Proc. R. Soc. London A* **1984**, *392*, 45−57.
(45) Zhan, Q.; Leger, J. R. Interferometric measurement of Berry's phase in space-variant polarization manipulations. *Opt. Commun.* **2002**, *213*, 241−245.
(46) Beijersbergen, M. W.; Coerwinkel, R. P. C.; Kristensen, M.; Woerdman, J. P. Helical-wavefront laser beams produced with a spiral phaseplate. *Opt. Commun.* **1994**, *112*, 321−327.
(47) Bazhenov, V. Yu.; Vasnetsov, M. V.; Soskin, M. S. Laser beams with screw dislocations in their wavefronts. *JETP Lett.* **1990**, *52*, 429−431.
(48) Heckenberg, N. R.; McDuff, R.; Smith, C. P.; White, A. G. Generation of optical phase singularities by computer-generated holograms. *Opt. Lett.* **1992**, *17*, 221−223.
(49) Genevet, P.; Lin, J.; Kats, M. A.; Capasso, F. Holographic Detection of the Orbital Angular Momentum of Light with Plasmonic Photodiodes. *Nat. Commun.* **2012**, *3*, 1278.
(50) Leith, E. N.; Upatnieks, J. Wavefront reconstruction and communication theory. *J. Opt. Soc. Am.* **1962**, *52*, 1123−1128.
(51) Grier, D. G. A revolution in optical manipulation. *Nature* **2003**, *424*, 810−816.
(52) Gabriel, C.; et al. Entangling Different Degrees of Freedom by Quadrature Squeezing Cylindrically Polarized Modes. *Phys. Rev. Lett.* **2011**, *106*, 060502.